

# Phosphorus Doped $\text{Zn}_{1-x}\text{Mg}_x\text{O}$ Nanowire Arrays

S. S. Lin,<sup>†</sup> J. I. Hong,<sup>†</sup> J. H. Song,<sup>†</sup> Y. Zhu,<sup>‡</sup> H. P. He,<sup>‡</sup> Z. Xu,<sup>‡</sup> Y. G. Wei,<sup>†</sup>  
Y. Ding,<sup>†</sup> R. L. Snyder,<sup>†</sup> and Z. L. Wang<sup>\*†</sup>

*School of Materials Science and Engineering, Georgia Institute of Technology, Atlanta, Georgia 30332-0245, and State Key Laboratory of Silicon Materials, Zhejiang University, Hangzhou, 310027, China*

Received June 29, 2009

## ABSTRACT

We demonstrate the growth of phosphorus doped  $\text{Zn}_{1-x}\text{Mg}_x\text{O}$  nanowire (NW) using pulsed laser deposition. For the first time, p-type  $\text{Zn}_{0.92}\text{Mg}_{0.08}\text{O}:\text{P}$  NWs are likely obtained in reference to atomic force microscopy based piezoelectric output measurements, X-ray photoelectron spectroscopy, and the transport property between the NWs and a n-type ZnO film. A shallow acceptor level of  $\sim 140$  meV is identified by temperature-dependent photoluminescence. A piezoelectric output of 60 mV on average has been received using the doped NWs. Besides a control on NW aspect ratio and density, band gap engineering has also been achieved by alloying with Mg to a content of  $x = 0.23$ . The alloyed NWs with controllable conductivity type have potential application in high-efficiency all-ZnO NWs based LED, high-output ZnO nanogenerator, and other optical or electrical devices.

Semiconductor nanowires (NWs) have a broad range of applications in electronics,<sup>1</sup> optoelectronics,<sup>2</sup> biosciences,<sup>3</sup> and energy sciences.<sup>4</sup> Nanowire light emitting diodes (LEDs), for example, have advantages over traditional light sources including lower energy consumption, longer lifetime, and improved robustness. Zinc oxide (ZnO) is a multifunctional material that not only has the great potential to fabricate high-efficiency violet-blue LEDs but also is a promising material to harvest solar and mechanical energy. Compared to GaN, a classical and commercialized blue-UV emitter, ZnO has several advantages such as twice the large exciton energy, availability of large-area single crystalline substrates, amenability to low-temperature growth, and high radiation resistance. Nevertheless, despite many efforts searching for a better acceptor dopant for ZnO,<sup>5–10</sup> p-type doping in ZnO is still difficult as it suffers from low stability, low acceptor solubility, severe donor compensation, and so forth.<sup>11</sup> Recently, there have been a few reports concerning p-type ZnO NWs<sup>12,13</sup> by the vapor phase deposition method, which have received particular attention since these NWs are single crystal and have the potential to improve the efficiency of all-ZnO-based LEDs.

p-Type NWs also show superior performance as a nanogenerator,<sup>14</sup> which utilizes a unique coupling of the semiconductive and piezoelectric properties of ZnO.<sup>4,15–17</sup> Previous experimental and theoretical studies revealed that

p-type NWs exhibit positive voltages outputs and n-type NWs exhibit negative voltages outputs;<sup>14</sup> and the p-type NWs give higher piezoelectric output. A nondestructive technique has been demonstrated to discriminate the conductivity type of the ZnO NWs using the signal from a nanogenerator.<sup>14,18</sup> As for nanopiezotronics,<sup>19</sup> conductivity type controlled n- and p- NWs allow us to construct a logic circuit based on the piezo-potential gated n-channel and p-channel field effect transistors (FETs) in analogy to the complementary metal oxide FETs that are widely used in today's electronics.

In addition, band gap engineering in ZnO NWs is also highly desirable since heterostructure<sup>20</sup> or quantum wells<sup>21</sup> should be incorporated into the LEDs structure to further enhance the quantum efficiency. p-Type alloyed  $\text{Zn}_{1-x}\text{Mg}_x\text{O}$  NWs can provide LEDs that emit a shorter wavelength compared to p-type ZnO NWs. The p-type  $\text{Zn}_{1-x}\text{Mg}_x\text{O}$  NWs, which play a critical role as an electron blocking layer, are highly desirable in the multiquantum well nano-LED. Up to now, there are no reports of growth of p-type  $\text{Zn}_{1-x}\text{Mg}_x\text{O}$  NWs.

In this paper, we present the growth of  $\text{Zn}_{1-x}\text{Mg}_x\text{O}$  NWs array by pulse laser deposition (PLD) without using a catalyst on popular substrates such as silicon and quartz. The p-type conductivity in  $\text{Zn}_{0.92}\text{Mg}_{0.08}\text{O}$  is likely received by doping with phosphorus. Phosphorus doped  $\text{Zn}_{1-x}\text{Mg}_x\text{O}$  NWs can produce a piezoelectric output voltage up to 60 mV, which is 6 times greater than that of the vapor-liquid-solid (VLS) grown n-type ZnO NWs.<sup>4</sup> The morphology, dimension, band gap, and/or conductivity type have been controlled through

\* To whom correspondence should be addressed. E-mail: zhong.wang@mse.gatech.edu.

<sup>†</sup> Georgia Institute of Technology.

<sup>‡</sup> Zhejiang University.

proper choice of experimental conditions. The newly fabricated p-type NWs may provide a new opportunity for fabricating NW-based LEDs, optoelectronic, electronic, and piezotronic devices, as well as high-output nanogenerators.

PLD is a popular technique for thin film deposition ever since its demonstration as growing high-quality superconductive thin films.<sup>22</sup> PLD can be used for deposition of a wide range of materials, such as ceramic oxides, nitride films, metallic films and superlattices. Recently, there is an interest in growing semiconductor NWs using this technique with the use of catalysts in some cases.<sup>23–25</sup> For our NW growth using PLD, a KrF excimer laser (Coherent Compex 205, wavelength of 248 nm) was used as the ablation source to focus on a ceramic target, and the incident fluence was approximately 3 J/cm<sup>2</sup>. The detailed target preparation process can be found in ref 10. All of the ZnO nanostructures are deposited on  $\sim 2 \times 2$  cm<sup>2</sup> Si(100) or polycrystalline quartz substrates with a typical growth time of 40 min. The morphology of the resultant product is uniform in an area of  $\sim 1 \times 1$  cm<sup>2</sup>, where the center is in line with the plume axis. As a proof-of-principle that the growth method is applicable to any doped or alloyed ZnO targets, a lithium-doped Zn<sub>0.95</sub>Mg<sub>0.05</sub>O (0.5 at.% doping concentration of Li) ceramic was used as the ablation target for investigating the effect of growth parameters. The key point for growing vertically aligned NWs is in situ fabrication of a textured ZnO buffer layer on a silicon substrate before switching to the condition for the growth of NWs.

The topology of the NW array can be controlled by four parameters, substrate temperature ( $T$ ), growth pressure, the flow ratio of argon and oxygen, and laser repetition frequency. At a laser repetition frequency of 5 Hz and a flowing mixture of Ar and O<sub>2</sub> at a flow ratio of 6:1 with a total pressure of 5.0 Torr, the SEM images of the NWs produced at a series of  $T$ s are shown in Figure 1a–d. At a  $T$  of 700 °C, a film with a rough surface was obtained (Figure 1a). When  $T$  was increased to 750 °C, NWs were formed with a typical length of  $\sim 800$  nm (Figure 1b). Longer NWs of lengths  $\sim 2$ – $3$   $\mu$ m were grown at 800 °C (Figure 1c). Further increasing  $T$  to 850 °C merged a few NWs together (Figure 1d). On the other hand, by fixing  $T$  at 800 °C, the dependence of the aspect ratio on the growth pressure was revealed. As the growth pressure increased to 6.0 Torr, slimmer NWs (Figure 1e) were formed, while larger diameter NWs were obtained at 4.0 Torr (Figure 1f). The aspect ratio can thus be controlled by adjusting the  $T$  and growth pressure.

Maintaining  $T$  at 800 °C, morphology tailoring was further demonstrated by first growing NWs at 5.0 Torr for 20 min then at 4.5 Torr for 20 min. The NWs have larger diameters at the top than at the bottom (Figure 2a), exhibiting a nail-shape morphology by adjusting experimental conditions. This morphology tailoring was reproducible and allows us to design complex heterostructures and p-n junctions (see below). For incorporating group-I or group-V elements as shallow acceptors, an oxygen rich condition is necessary.<sup>26</sup> Figure 2b,c shows NW arrays grown under pure argon and mixed argon/oxygen (6:1) atmospheres, respectively. It is shown that adding oxygen into the chamber makes the

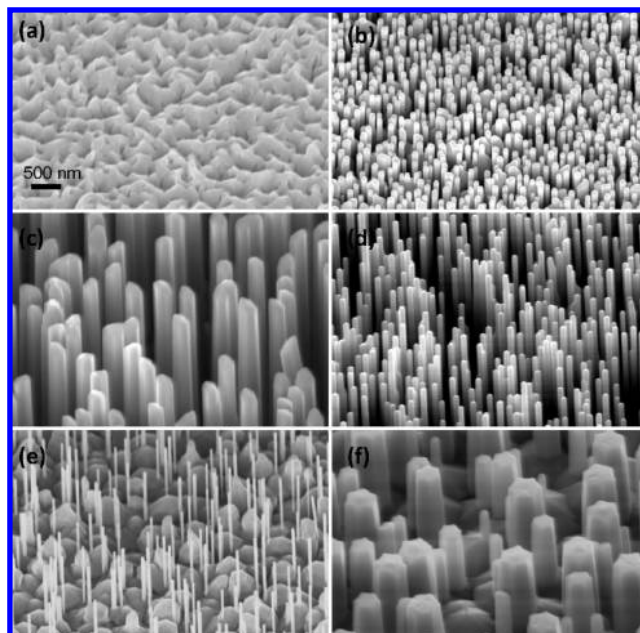


**Figure 1.** SEM tilted views of the NWs grown at (a) 700, (b) 750, (c) 800, (d) 850 °C and the growth pressure was 5 Torr. (e,f) NWs array grown at 6.0 and 4.0 Torr at 800 °C. All of the images use one scale bar of 500 nm. A mixture of argon and oxygen with flow ratio of 6 is used as working gas and the laser repetition frequency is 5 Hz. The target is lithium-doped Zn<sub>0.95</sub>Mg<sub>0.05</sub>O (0.5 at.% doping concentration of Li).

diameters of the NWs larger and the length smaller. The top view of the NWs in Figure 2c is shown in Figure 2d, revealing that the NWs are highly perpendicular to the substrate. The corresponding  $\theta$ – $2\theta$  XRD spectra are shown in Figure 2e, in which only ZnO (0002), (0004), and silicon (400) peaks can be found. The inset in Figure 2e displays the rocking curve of ZnO (0002) peak with the full width at half-maximum (fwhm) of 136'', demonstrating that NWs grew along  $c$ -axis direction with a perfectly vertical alignment. Although the density and aspect ratio of the NWs varies for different doped or alloyed targets, perfectly aligned NW arrays can still be obtained. Figure 2f presents SEM image of NWs fabricated from a target containing 1.5 at.% Na and Figure 2g displays the top view of the NWs. As seen from the inset of Figure 2g, the NWs grow from the tip of hexagonal bases, which may indicate a diffusion mechanism of formation of the NWs.<sup>27</sup> Up to now, we have confirmed that this method for growing NWs is highly reproducible and applicable to any ZnO targets including doped or alloyed ones. Furthermore, it is demonstrated that the NW array can be produced at a larger scale and on transparent substrates, such as polycrystalline quartz (see more in Supporting Information Figures S1 and S2).

Substituting Mg at the Zn sites can increase the band gap to approximately 4.0 eV while still maintaining the wurtzite structure.<sup>28</sup> Because of the nonequilibrium process caused by laser heating under a short-pulse on the order of nanoseconds, the ability to replicate the composition of the source in the deposited products is perhaps the greatest benefit of PLD.<sup>22</sup> Epitaxial wurtzite Zn<sub>1-x</sub>Mg<sub>x</sub>O thin films have been realized using PLD with  $x$  as large as 0.35 by

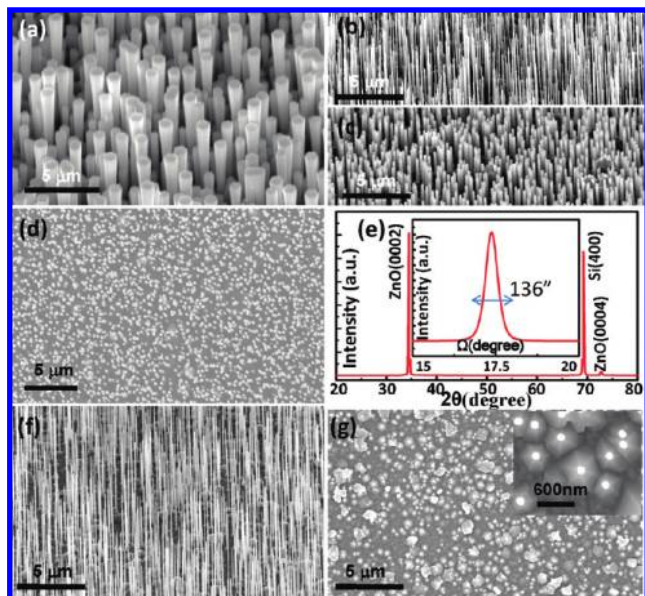


**Figure 2.** (a) NWs prepared at 5.0 Torr with an Ar/O<sub>2</sub> flow ratio of 6 for 20 min followed by at 4.5 Torr for 20 min. These NWs show a larger diameter at the top compared with that at the bottom. NWs grown under (b) 5.0 Torr of pure argon. (c) 5.0 Torr at Ar/O<sub>2</sub> flow ratio of 6. The comparison between (b) and (c) reveals that the aspect ratio becomes smaller when oxygen partial pressure is higher. (d) Top view of the NWs of (c), revealing that the NWs are perfectly vertical to the silicon substrate. (e) The corresponding XRD spectra. Inset, rocking curve of (0002) peak shows a small fwhm value of 136''. From panels a–e, the target is Zn<sub>0.95</sub>Mg<sub>0.05</sub>O:Li ceramic (0.5 at.% doping concentration of Li). (f) NWs produced from another target containing 1.5 at.% Na under 5.0 Torr with argon/oxygen flow ratio of 6. (g) Top view of NWs in (f). Inset, magnified top view of NWs, which appear as bright white spots and grow from hexagonal bases.

Ohtomo et al.<sup>28</sup> Here, uniform Zn<sub>1-x</sub>Mg<sub>x</sub>O NWs with a series of  $x$  values can be obtained simply through ablating a Zn<sub>0.9</sub>Mg<sub>0.1</sub>O target under different background growth pressure at Ar/O<sub>2</sub> flow ratio of 6. We found that the doping concentration is highly related to the growth pressure and this fact adds more flexibility to control the doping level. Maintaining  $T$  at 800 °C, the densities of NWs are controllable through simply adjusting the laser repetition frequency. Keeping the growth pressure constant at 4.5 Torr, the NWs deposited under laser repetition frequency of 1, 3, 5 Hz are shown in Figure 3a–c, respectively. The NWs density continuously increases as the laser repetition frequency is raised. Energy dispersive X-ray spectroscopy (EDX) reveals that the Mg content is ~0, 2, 8, 19, and 23 for the Zn<sub>1-x</sub>Mg<sub>x</sub>O NWs grown at the pressure of 5.0, 4.5, 4.0, 3.5, 3.0 Torr, respectively (Supporting Information Figure S3). Typically, Figure 3d shows the Zn<sub>1-x</sub>Mg<sub>x</sub>O NWs grown at 4.0 Torr, the EDX spectrum of which is displayed in Figure 3e with a readily detected Mg peak.

Photoluminescence (PL) measurements were performed using a 325 nm He–Cd laser as the excitation source on a FLS920 (Edinburgh Instruments) fluorescence spectrometer. Figure 3f illustrates the room temperature band-edge PL of Zn<sub>0.98</sub>Mg<sub>0.02</sub>O, Zn<sub>0.92</sub>Mg<sub>0.08</sub>O, Zn<sub>0.81</sub>Mg<sub>0.19</sub>O, and Zn<sub>0.77</sub>Mg<sub>0.23</sub>O NWs. The inset of Figure 3f displays a typical PL spectrum for the Zn<sub>0.98</sub>Mg<sub>0.02</sub>O NWs and the deep level

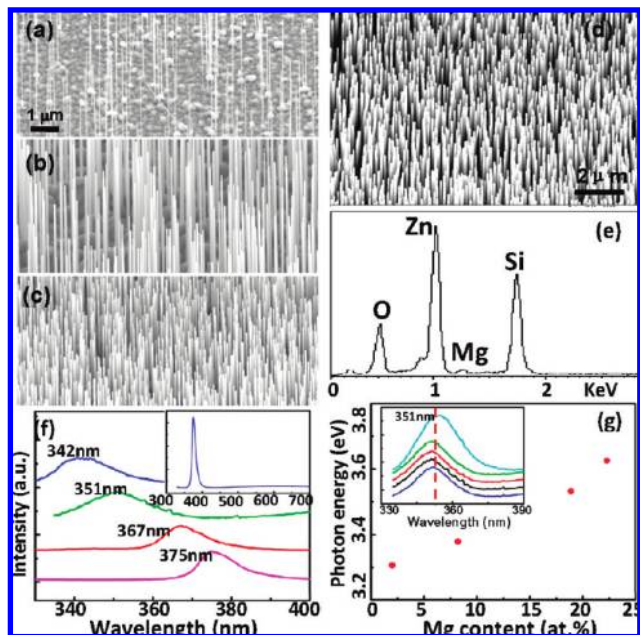


**Figure 3.** SEM views of Zn<sub>1-x</sub>Mg<sub>x</sub>O NWs produced from Zn<sub>0.9</sub>Mg<sub>0.1</sub>O target under the laser repetition frequency of (a) 1, (b) 3, and (c) 5 Hz. Scale bar in (a–c) is 1 μm. (d) Typical SEM view of Zn<sub>1-x</sub>Mg<sub>x</sub>O NWs grown at 4.0 Torr (e) Corresponding EDS spectrum of the NWs in (d). (f) Room temperature band-edge PL spectra of NWs array fabricated at 4.5, 4.0, 3.5, and 3.0 Torr (from bottom to top). Right-up inset: Typical PL spectra of NWs array fabricated at 4.5 Torr. (g) Dependence of band gap on the Mg content in the NWs. Left-upper inset: band-edge PL spectra for five arbitrary positions in the NWs array fabricated at 3.5 Torr.

defect emission is very weak, indicating free of oxygen vacancy.<sup>29</sup> As the Mg content increases, the PL peak shifts systematically to shorter wavelength (higher energy). The optical band gap of the Zn<sub>1-x</sub>Mg<sub>x</sub>O NWs increases almost linearly as the Mg content increases (Figure 3g). The upper-left inset in Figure 3g illustrates band-edge PL spectra of Zn<sub>0.81</sub>Mg<sub>0.19</sub>O NWs on the five random and scattered positions of the substrate (in a area of 1 cm<sup>2</sup>); all of the PL peaks locate at ~351 nm with only a small deviation, confirming that the Mg content is fairly uniform across the NWs array.

p-Type Zn<sub>1-x</sub>Mg<sub>x</sub>O NWs are highly desirable because they have the potential to offer a fundamental unit that is controlled in band gap and conductivity type. Furthermore, reducing the background electron concentration via Mg alloying facilitates transformation of ZnO NWs into p-type conductivity.<sup>30–32</sup> A target containing 4 at.% phosphorus and 10 at.% Mg was used to carry out phosphorus-doping experiments at 800 °C under a series of growth pressures and an oxygen rich condition at Ar/O<sub>2</sub> flow ratio of 6. SEM image of NWs grown at 4.0 Torr are shown in Figure 4a, doping phosphorus into the ZnO lattice makes the NWs surface rough as a result of induced strain<sup>12</sup> (more evidence about the morphology change by phosphorus doping can be found in Supporting Information Figure S4). For the NWs grown at 4.0 Torr, high-resolution X-ray photoelectron spectroscopy (XPS) data of Mg 1s core-level identified that Mg has been alloyed into the NWs and quantitative analysis reveals the Mg content is ~8 at.%. Systematic XPS investigations were performed to uncover the trend of

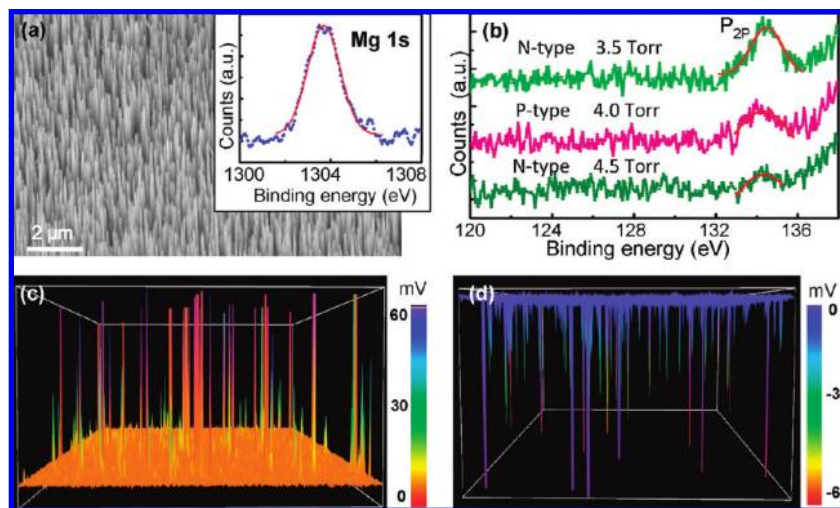


**Figure 4.** (a) Typical SEM image of phosphorus-doped  $\text{Zn}_{1-x}\text{Mg}_x\text{O}$  NWs prepared at 4.0 Torr with Ar/O<sub>2</sub> flow ratio of 6. (Inset) Mg 1s high-resolution XPS scan. (b) High-resolution XPS spectra of P<sub>2p</sub> for the NWs array prepared under a series of pressure (from top to bottom: 3.3, 4.0, 4.5 Torr). (c) Three-dimensional piezoelectric output of the NWs array prepared at 4.0 Torr. The area is 20  $\mu\text{m} \times 20 \mu\text{m}$ . (d) Typical three-dimensional piezoelectric outputs of the NWs array grown under 3.3 or 4.5 Torr, when scanned in contact mode by conductive AFM. The area is 20  $\mu\text{m} \times 20 \mu\text{m}$ .

phosphorus incorporation in the NWs. Since the oxygen concentration is severely influenced by oxygen absorptions, herein, the phosphorus concentration refers to the percentage of the atomic ratio of P to Zn in the NWs. Figure 4b reveals that P<sub>2p</sub> core-level peak intensity in the high-resolution XPS spectrum decreases as the growth pressure increases. It is worth noting that the Zn 2P core level signal intensity increases slightly for the sample grown at higher growth pressure (Supporting Information Figure S5). Thus, the phosphorus doping concentration decreases as the growth pressure increases, which is reasonable by analogy with Mg alloying. The binding energy of the P<sub>2p</sub> core-level peak locates at  $\sim 134.4$  eV, which is believed to originate from P–O bond in the NWs analogous to the film counterpart.<sup>33</sup>

The piezoelectric responses tests were adopted to discriminate the conductivity type of the phosphorus-doped ZnO NWs.<sup>14,18</sup> The piezoelectric responses of the NWs were measured by using an atomic force microscope (AFM) (Molecular Force Probe MFP-ED from Asylum Research) with a Pt-coated Si tip. In the AFM contact mode, a constant normal force of 80 nN was maintained between the tip and NWs. A voltage drop across an external load of 500 M $\Omega$  connected to the AFM tip was continuously monitored when the tip scanned across the sample. Under repeated measurements, the NWs grown at 4.0 Torr output positive voltages (Figure 4c), indicating a p-type conductivity. For the NWs grown at 3.3 or 4.5 Torr, the piezoelectric outputs are negative (a typical result is displayed in Figure 4d), corresponding to n-type conductivity. The negative output voltage can be boosted up to  $\sim 60$  meV (Figure 4d), which shows that the electron concentration is reduced favorable for high potential output.<sup>34</sup> The P<sub>Zn</sub>-2V<sub>Zn</sub> complex, a shallow acceptor with low-formation energy under oxygen rich conditions, is believed to be the cause of the p-type conductivity.<sup>35</sup> It is well known that acceptor doping increases the Madelung energy of the lattice, so an appropriate doping level is critical to optimize the Madelung energy and obtain p-type conduc-

tivity.<sup>9</sup> The doping level for the NWs grown at 4.5 Torr is low and the ionized holes can not completely compensate the electrons, resulting in n-type conductivity. On the other hand, the abundant phosphorus in the NWs grown at 3.3 Torr tends to form P<sub>Zn</sub> antisite donors or P<sub>O</sub> deep acceptors that contribute little to p-type conductivity, therefore, the P<sub>Zn</sub> antisite donors suppress p-type conductivity, possibly leading to n-type conductivity. The severe competition between the deep acceptor/donor and shallow acceptor is common for acceptor doped ZnO films,<sup>6,8,10,36–39</sup> revealing that p-type conductivity in  $\text{Zn}_{1-x}\text{Mg}_x\text{O}$  NWs is possible only within a proper range of doping concentration. Experimentally we found that target materials containing phosphorus with low content (2 at.%) or high content (6 at.%) and Mg content of 10 at.% produced n-type NWs at 4.0 Torr, supporting that appropriate phosphorus doping concentration is vital to p-type conductivity.

The PL spectrum of p-type  $\text{Zn}_{0.92}\text{Mg}_{0.08}\text{O}$  NWs at 16K contains a strong band-edge emission and a weak red-emission around 680 nm (Figure 5a). Two bands locating around 357 nm (3.473 eV) and 364 nm (3.407 eV) were found in the band-edge emission displayed in the inset of Figure 5a. The band around 357 nm is reasonably attributed to a neutral acceptor bound exciton (A<sup>0</sup>X), considering the phosphorus acceptor doping. The band around 364 nm experiences an obvious blue shift first from 16 to 80 K then a red shift as the temperature increases from 80 to 140 K, as indicated in the temperature-dependent PL spectra shown in Figure 5b. The band around 364 nm at 16 K is attributed to donor–acceptor pair (DAP) transition and it evolves into electron-to-neutral acceptor (eA<sup>0</sup>) transition at 80 K under the gradual ionization of donor. The dependence of eA<sup>0</sup> energy on temperature is given by  $E_{eA^0} = E_g - E_A + kT/2$ , where  $E_g$ ,  $E_A$ , and  $k$  are the band gap, acceptor binding energy, and Boltzmann constant, respectively. Considering the difference ( $\sim 20$  meV) between the free-exciton (FX) emission and the A<sup>0</sup>X<sup>39,40</sup> and taking the position of A<sup>0</sup>X

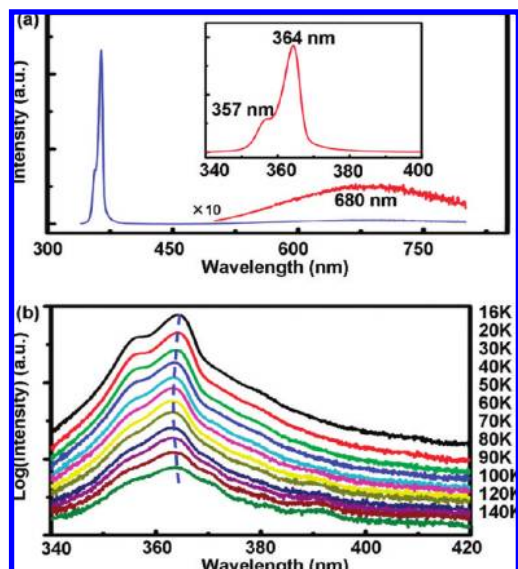


**Figure 5.** (a) PL spectrum of the p-type  $\text{Zn}_{0.92}\text{Mg}_{0.08}\text{O:P}$  NWs array at 16 K, which was prepared under a growth pressure of 4.0 Torr. (Inset) The band-edge emissions at 16 K. (b) Temperature-dependent photoluminescence spectra of these NWs; the blue dotted line indicates that the emission line at 364 nm undergoes an obvious blue shift (from 16 to 80 K) and a subsequent red shift (80 to 140 K), which is typical for a DAP emission.

and  $eA^0$  at 80 K, the binding energy of the phosphorus-related acceptor is deduced to be  $\sim 140$  meV. This shallow acceptor is ascribed to  $\text{P}_{\text{Zn}}-2\text{V}_{\text{Zn}}$  configuration.<sup>35</sup> On the other hand, the deep defect emission around 680 nm should be induced by  $\text{P}_\text{O}$  configuration as it is absent in the undoped  $\text{Zn}_{1-x}\text{Mg}_x\text{O}$  and ZnO NWs.<sup>12</sup> A narrow growth window of p-type conductivity is a result of the competition between the shallow acceptor and deep acceptor, which is in consistence with the piezoelectric output and XPS measurements. Moreover, the dominating DAP emission in the band-edge PL is in line with the p-type conductivity in  $\text{Zn}_{0.92}\text{Mg}_{0.08}\text{O:P}$  NWs.

Correlating the AFM outputs with the electrical properties tuned by doping can be further explored by the Fermi level in the produced NWs through valence band (VB) XPS. Figure 6a shows the VB XPS spectra of  $\text{Zn}_{0.92}\text{Mg}_{0.08}\text{O:P}$  and n-type ZnO NWs, which are all prepared at 4.0 Torr and 800 °C. For pure ZnO NWs, the peak around 10.6 eV and the broadband around 7.6 and 5.0 eV are known to have originated from Zn 3d, mixed Zn 4s-O 2p and O 2p states, respectively.<sup>41</sup> By extrapolating the leading edge of the O 2p-derived valence band to its intersection with background counts, the positions of the Fermi level with respect to the valence band maximum (VBM) was determined, as shown in the inset of Figure 6a. The Fermi level is located at 3.1 eV above the VBM for the pure ZnO NWs while it is only 0.9 eV for the  $\text{Zn}_{0.92}\text{Mg}_{0.08}\text{O:P}$  NWs. This is consistent with the conductivity type measurements by AFM. Filling in the gap among the NWs with poly(methyl methacrylate) (PMMA) and exposing the tips of the NWs by partly etching the PMMA through an  $\text{O}_2$  plasma, a junction between the NWs and the underlying n-type pure ZnO layer is formed. The electrodes for the p-type NWs are formed by depositing 20

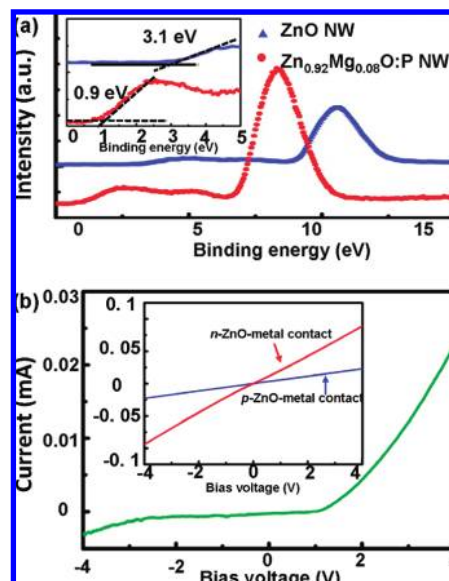


**Figure 6.** (a) VB XPS spectra pure ZnO NWs and of  $\text{Zn}_{0.92}\text{Mg}_{0.08}\text{O:P}$  NWs. (Inset) VB XPS spectra near the Fermi level shows the Fermi level locates at 3.1 and 0.9 eV above VBM for pure ZnO NWs and  $\text{Zn}_{0.92}\text{Mg}_{0.08}\text{O:P}$  NWs, respectively. (b)  $I-V$  characteristic of junction between p-type  $\text{Zn}_{0.92}\text{Mg}_{0.08}\text{O:P}$  NWs and underlying n-type ZnO layer. (Inset) The electrical properties of metal contact to on the p-type NWs and n-type pure ZnO layer.

nm Ni and then 100 nm Au through e-beam evaporation while indium dots are annealed to form contacts with the n-type layer. The linear  $I-V$  dependences between the electrodes and p/n layers confirm ohmic contacts (inset of Figure 6b). The rectifying shape  $I-V$  characteristic between the ZnO film and  $\text{Zn}_{0.92}\text{Mg}_{0.08}\text{O:P}$  NWs (Figure 6b) reveals that a p-n junction is formed between the n-type ZnO film and the  $\text{Zn}_{0.92}\text{Mg}_{0.08}\text{O:P}$  NWs and strongly demonstrates the p-type conductivity of the  $\text{Zn}_{0.92}\text{Mg}_{0.08}\text{O:P}$  NWs array.

In summary, using PLD we have presented a systematic study on how to control the morphology, density, and dimension of alloyed ZnO NW arrays. Through adjusting the phosphorus doping concentration, the p-type conductivity is likely to present in alloyed  $\text{Zn}_{0.92}\text{Mg}_{0.08}\text{O}$  NWs. Our study proves that a specifically controlled doping concentration of phosphorus is vital to achieve p-type conductivity. The band gap of the NWs can be increased up to 3.63 eV ( $x = 0.23$ ) as a result of substituting Zn by Mg. This study shows the potential of simultaneously controlling the doping concentration and tuning band gap of ZnO NWs for the purposes of high-efficiency all-ZnO based LED, high-output nanogenerators and other optical or electrical devices.

**Acknowledgment.** The authors thank J. X. Wu for assistance of valence-band X-ray photoelectron spectroscopy tests and X. Q. Gu for assistance of the temperature-dependent photoluminescence measurements. This research was supported by DARPA (Army/AMOCOM/REDSTONE AR, W31P4Q-08-1-0009), BESDOE (DE-FG-02-07ER46394), AirForce Office (FA9550-08-1-0046), DARPA/AROW911NF-08-1-0249, KAUST Global Research Partnership. S.S.L. thanks the partial fellowship supported by the China Scholarship Council (CSC) (No. 20083019).

**Supporting Information Available:** This material is available free of charge via the Internet at <http://pubs.acs.org>.

## References

- (1) Cui, Y.; Lieber, C. M. *Science* **2001**, *291*, 851.
- (2) (a) Duan, X. F.; Huang, Y.; Cui, Y.; Wang, J. F.; Lieber, C. M. *Nature* **2001**, *409*, 66. (b) Gudiksen, S. M.; Lathon, J. L.; Wang, J. F.; Smith, D. C.; Lieber, C. M. *Nature* **2002**, *415*, 617.
- (3) Cui, Y.; Wei, Q. Q.; Park, H. K.; Lieber, C. M. *Science* **2001**, *293*, 1289.
- (4) Wang, Z. L.; Song, J. H. *Science* **2006**, *312*, 242.
- (5) Tsukazaki, A.; Ohtomo, A.; Onuma, T.; Ohtani, M.; Makino, T.; Sumiya, M.; Ohtani, K.; Chichibu, S.; Fuke, S.; Segawa, Y.; Ohno, H.; Koinuma, H.; Kawasaki, M. *Nat. Mater.* **2005**, *4*, 42.
- (6) Allenic, A.; Guo, W.; Chen, Y. B.; Pan, X. Q.; Che, Y.; Hu, Z. D.; Liu, B. *Adv. Mater.* **2007**, *19*, 3333.
- (7) Ryu, R. Y.; Lubguban, J. A.; Lee, T. S.; White, H. W.; Jeong, T. S.; Youn, C. J.; Kim, B. J. *Appl. Phys. Lett.* **2007**, *90*, 131115.
- (8) Xiu, F. X.; Yang, Z.; Mandalapu, L. J.; Zhao, D. T.; Liu, J. L. *Appl. Phys. Lett.* **2005**, *87*, 252102.
- (9) Zeng, Y. J.; Ye, Z. Z.; Xu, W. Z.; Li, D. Y.; Lu, J. G.; Zhu, L. P.; Zhao, B. H. *Appl. Phys. Lett.* **2006**, *88*, 062107.
- (10) Lin, S. S.; Ye, Z. Z.; Lu, J. G.; He, H. P.; Chen, L. X.; Gu, X. Q.; Huang, J. Y.; Zhu, L. P.; Zhao, B. H. *J. Phys. D: Appl. Phys.* **2008**, *41*, 155114.
- (11) Look, D. C.; Clfflin, B. *Phys. Status Solidi B* **2004**, *241*, 624.
- (12) Xiang, B.; Wang, P. W.; Zhang, X. Z.; Dayeh, S. A.; Aplin, D. P. R.; Soci, C.; Yu, D. P.; Wang, D. L. *Nano. Lett.* **2007**, *7*, 323.
- (13) Yuan, G. D.; Zhang, W. J.; Jie, J. S.; Fan, X.; Zapien, J. A.; Leung, Y. H.; Luo, B. J.; Wang, P. F.; Lee, C. S.; Lee, S. T. *Nano. Lett.* **2008**, *8*, 2591.
- (14) Lu, M.-P.; Song, J. H.; Lu, M.-Y.; Chen, M.-T.; Gao, Y. F.; Chen, L.-J.; Wang, Z. L. *Nano. Lett.* **2009**, *9*, 1223.
- (15) Wang, X. D.; Song, J. H.; Liu, J.; Wang, Z. L. *Science* **2007**, *316*, 102.
- (16) Qin, Y.; Wang, X. D.; Wang, Z. L. *Nature* **2008**, *451*, 809.
- (17) Yang, R.; Qin, Y.; Dai, L.; Wang, Z. L. *Nat. Nanotechnol.* **2009**, *4*, 34.
- (18) Lin, S. S.; Song, J. H.; Lu, Y. F.; Wang, Z. L. *Nanotechnology*, **2009**, *20*, 365703.
- (19) Wang, Z. L. *Adv. Mater.* **2007**, *19*, 889.
- (20) Nakamura, S.; Mukai, T.; Senoh, M. *Appl. Phys. Lett.* **1994**, *64*, 1687. Chu, S.; Olmedo, M.; Yang, Z.; Kong, J. Y.; Liu, J. L. *Appl. Phys. Lett.* **2008**, *93*, 181106.
- (21) (a) Ryu, Y. R.; Lee, T.-S.; Lubguban, J. A.; White, H. W.; Kim, B.-J.; Park, Y.-S.; Youn, C.-J. *Appl. Phys. Lett.* **2006**, *88*, 241108. (b) Ye, Z. Z.; Lin, S. S.; He, H. P.; Gu, X. Q.; Chen, L. X.; Lu, J. G.; Huang, J. Y.; Zhu, L. P.; Wang, L.; Zhang, Y. Z.; Li, X. H. *J. Semicond. (in Chinese)* **2008**, *29*, 1433.
- (22) (a) Dijkamp, D.; Venkatesan, T.; Wu, X. D.; Shaheen, S. A.; Jisrawi, N.; M-L, Y. H.; Mclean, W. L.; Croft, M. *Science* **1987**, *51*, 619. (b) Norton, D. P.; Chakoumakos, B. C.; Budai, J. D.; Lowndes, D. H.; Sales, B. C.; Thompson, J. R.; Chirsten, D. K. *Science* **1994**, *265*, 2074. (c) Norton, D. P.; Goyal, A.; Budai, J. D.; Christen, D. K.; Kroeger, D. M.; Specht, E. D.; He, Q.; Saffian, B.; Paranthaman, M.; Klabunde, C. E.; Lee, D. F.; Sales, B. C.; List, F. A. *Science* **1996**, *274*, 755.
- (23) (a) Morales, A. M.; Lieber, C. M. *Science* **1998**, *279*, 208. (b) Duan, X. F.; Lieber, C. M. *J. Am. Chem. Soc.* **2000**, *122*, 188.
- (24) Lorenz, M.; Kaidashev, E. M.; Rahm, A.; Nobis, T.; Lenzner, J.; Wagner, G.; Spemann, D.; Hochmuth, H.; Grudmann, M. *Appl. Phys. Lett.* **2005**, *86*, 143113.
- (25) (a) Sun, Y.; Fuge, G. M.; Ashfold, M. N.R. *Chem. Phys. Lett.* **2004**, *396*, 21. (b) Tien, L. C.; Pearton, S. J.; Norton, D. P.; Ren, F. *J. Mater. Sci.* **2008**, *43*, 6925.
- (26) (a) Park, C. H.; Zhang, S. B.; Wei, S.-H. *Phys. Rev. B* **2002**, *66*, 073202. (b) Qin, R.; Zheng, J. X.; Lu, J.; Wang, L.; Lai, L.; Luo, G. F.; Zhou, J.; Li, H.; Gao, Z. X.; Li, G. P.; Mei, W. N. *J. Phys. Chem. C* **2009**, *113*, 9541.
- (27) Jensen, L. E.; Bjrk, M. T.; Jeppesen, S.; Persson, A. I.; Ohlsson, B. J.; Samuelson, L. *Nano Lett.* **2004**, *4*, 1961.
- (28) Ohtomo, A.; Kawasaki, M.; Koida, T.; Masubuchi, K.; Koinuma, H.; Sakurai, Y.; Yoshida, Y.; Yasuda, T.; Segawa, Y. *Appl. Phys. Lett.* **1998**, *72*, 2466.
- (29) Vanheusden, K.; Warren, W. L.; Seager, C. H.; Tallant, D. R.; Voigt, J. A.; Gnade, B. E. *J. Appl. Phys.* **1996**, *79*, 7983.
- (30) Ip, K.; Heo, Y. W.; Norton, D. P.; Pearton, S. J.; LaRoche, J. P.; Ben, F. *Appl. Phys. Lett.* **2004**, *85*, 1169.
- (31) Wang, P.; Chen, N.; Yin, Z.; Dai, R.; Bai, Y. *Appl. Phys. Lett.* **2006**, *89*, 202102.
- (32) Li, Y. F.; Yao, B.; Lu, Y. M.; Wei, Z. P.; Gai, Y. Q.; Zheng, C. J.; Zhang, Z. Z.; Li, B. H.; Shen, D. Z.; Fan, X. W. *Appl. Phys. Lett.* **2007**, *91*, 232115.
- (33) Kim, K.-K.; Kim, H.-S.; Hwang, D.-K.; Lim, J.-H.; Park, S.-J. *Appl. Phys. Lett.* **2003**, *83*, 63.
- (34) Liu, J.; Fei, P.; Song, J. H.; Wang, X. D.; Lao, C. S.; Tummala, R.; Wang, Z. L. *Nano Lett.* **2008**, *8*, 328.
- (35) (a) Limpijumng, S.; Zhang, S. B.; Wei, S. -H.; Park, C. H. *Phys. Rev. Lett.* **2004**, *92*, 155504. (b) Lee, W. J.; Kang, J. G.; Chang, K. J. *Phys. Rev. B* **2006**, *73*, 024117.
- (36) Heo, Y. W.; Park, S. J.; Ip, K.; Pearton, S. J.; Norton, D. P. *Appl. Phys. Lett.* **2003**, *83*, 1128.
- (37) Xiu, F. X.; Yang, Z.; Mandalapu, L. J.; Liu, J. L. *Appl. Phys. Lett.* **2006**, *88*, 152116.
- (38) Zhu, Y.; Lin, S. S.; Zhang, Y. Z.; Ye, Z. Z.; Lu, Y. F.; Lu, J. G.; Zhao, B. H. *Appl. Surf. Sci.* **2009**, *255*, 6201.
- (39) Hwang, D. K.; Kim, H. S.; Lim, J. H.; Oh, J. Y.; Yang, J. H.; Park, S. J.; Kim, K. K.; Look, D. C.; Park, Y. S. *Appl. Phys. Lett.* **2005**, *86*, 151917.
- (40) Meyer, B. K.; Sann, J.; Lautenschläger, S.; Wagner, M. R.; Hoffmann, A. *Phys. Rev. B* **2007**, *76*, 184120.
- (41) Girard, R. T.; Tjernberg, O.; Chiaia, G.; Soderholm, S.; Karlsson, U. O.; Wigren, C.; Nylen, H.; Lindau, I. *Surf. Sci.* **1997**, *373*, 409.

NL902067A